Original Article

MOLECULAR METABOLISM

# Crosstalk between corepressor NRIP1 and cAMP signaling on adipocyte thermogenic programming

**Emmanouela Tsagkaraki [1,**], Adilson Guilherme [1], Sarah M. Nicoloro [1], Mark Kelly [1], Lawrence M. Lifshitz [1], Hui Wang [1], Kyounghee Min [1], Leslie A. Rowland [1], Kaltinaitis B. Santos [1], Nicole Wetoska [1], Randall H. Friedline [1,2], Stacy A. Maitland [3], Min Chen [4], Lee S. Weinstein [4], Scot A. Wolfe [3,5], Jason K. Kim [1,2], Michael P. Czech [1,*]**

## ABSTRACT

**Objectives:** Nuclear receptor interacting protein 1 (NRIP1) suppresses energy expenditure via repression of nuclear receptors, and its depletion markedly elevates uncoupled respiration in mouse and human adipocytes. We tested whether NRIP1 deficient adipocytes implanted into obese mice would enhance whole body metabolism. Since β-adrenergic signaling through cAMP strongly promotes adipocyte thermogenesis, we tested whether the effects of NRIP1 knock-out (NRIP1KO) require the cAMP pathway.

**Methods:** NRIP1KO adipocytes were implanted in recipient high-fat diet (HFD) fed mice and metabolic cage studies conducted. The *Nrip1* gene was disrupted by CRISPR in primary preadipocytes isolated from control vs adipose selective GsαKO (cAdGsαKO) mice prior to differentiation to adipocytes. Protein kinase A inhibitor was also used.

**Results:** Implanting NRIP1KO adipocytes into HFD fed mice enhanced whole-body glucose tolerance by increasing insulin sensitivity, reducing adiposity, and enhancing energy expenditure in the recipients. NRIP1 depletion in both control and GsαKO adipocytes was equally effective in upregulating uncoupling protein 1 (UCP1) and adipocyte beiging, while β-adrenergic signaling by CL 316,243 was abolished in GsαKO adipocytes. Combining NRIP1KO with CL 316,243 treatment synergistically increased *Ucp1* gene expression and increased the adipocyte subpopulation responsive to beiging. Estrogen-related receptor α (ERRα) was dispensable for UCP1 upregulation by NRIPKO.

**Conclusions:** The thermogenic effect of NRIP1 depletion in adipocytes causes systemic enhancement of energy expenditure when such adipocytes are implanted into obese mice. Furthermore, NRIP1KO acts independently but cooperatively with the cAMP pathway in mediating its effect on adipocyte beiging.



**Keywords** Diabetes; Obesity; Adipose tissue; Adrenergic signaling; CRISPR; Implant

## 1. INTRODUCTION

Cell therapies have been successfully used in multiple fields of medicine such as oncology [1—4], yet are still far from clinical application in type 2 diabetes and obesity. Nonetheless, preclinical studies indicate the strong potential of adipocytes to be used as cell therapy vehicles, as adipocyte dysfunctions are linked with the pathogenesis of disrupted systemic glucose and lipid homeostasis [5—10]. Furthermore, numerous studies have shown efficacy of implanting thermogenic brown adipose tissue into obese mice to improve glucose tolerance [11—14]. More recently, CRISPR-based gene editing methods have been used to enhance the thermogenic phenotype of white adipocytes, which in turn have proved effective in enhancing systemic metabolic health when implanted into HFD fed mice [15,16]. Such studies from our laboratory targeted the thermogenic repressor *Nrip1* gene to upregulate UCP1 and other genes of the thermogenic program in mouse and human adipocytes prior to implantation [15,17,18]. While in other cell types, NRIP1 is known to display both corepressor and coactivator functions, in adipocytes it has been reported to interact with and negatively regulate PPARα and PPARγ as well as retinoid receptors and estrogen-related receptors that are transcriptional regulators of fat accumulation and thermogenesis [19—24]. NRIP1-

[1]Program in Molecular Medicine, University of Massachusetts Chan Medical School, Worcester, MA 01605, USA [2]Division of Endocrinology, Metabolism and Diabetes, Department of Medicine, University of Massachusetts Chan Medical School, Worcester, MA 01605, USA [3]Department of Molecular, Cell and Cancer Biology, University of Massachusetts Chan Medical School, Worcester, MA 01605, USA [4]Metabolic Diseases Branch, NIDDK, NIH, Bethesda, MD, 20892-1752, USA [5]Li Weibo Institute for Rare Diseases Research, University of Massachusetts Chan Medical School, Worcester, MA 01605, USA

*Corresponding author. 373 Plantation Street, Program in Molecular Medicine, University of Massachusetts Medical School, Worcester, MA 01605, USA. Fax: +1 508 856 1617. E-mail: michael.czech@umassmed.edu (M.P. Czech).

**Corresponding author. 373 Plantation Street, Program in Molecular Medicine, University of Massachusetts Medical School, Worcester, MA 01605, USA. Fax: +1 508 856 1617. E-mail: emmanouela.tsagkaraki@umassmed.edu (E. Tsagkaraki).

Received March 27, 2023 • Revision received July 13, 2023 • Accepted July 14, 2023 • Available online 22 July 2023

https://doi.org/10.1016/j.molmet.2023.101780

 

depleted adipocytes display increases in insulin-induced glucose uptake, fatty acid oxidation, energy expenditure and oxygen consumption, particularly in response to catecholamines [15,17,18,20,22,24]. Adipocyte implants have been reported to form fat pads that are fully innervated and vascularized within about 9 weeks from implantation [25,26]. In our studies, all implants including those containing control (NTC) and NRIP1KO adipocytes were observed to successfully engraft and are retrieved at the end of the experiments. No signs of rejection, other inflammatory or immune reactions or necrotic tissue have been observed. These CRISPR-engineered human and mouse adipocytes continued to consistently display the beige-like phenotype when retrieved four months following their successful implantation and engraftment [15].

In mammalian brown adipose tissue, a classical mechanism of thermogenic induction in response to activation of the sympathetic nervous system by cold exposure is mediated via β-adrenergic signaling. This pathway involves release of norepinephrine which stimulates G-protein coupled receptors, including the β1, β2 receptors and the adipocyte-specific β3 receptor that act through the Gsα protein [10,27–31]. Activation of this pathway leads to stimulation of adenylyl cyclase and cAMP synthesis, which activates protein kinase A (PKA) and phosphorylation of downstream targets that induce thermogenic programming. These targets include phosphorylation and activation of p38 protein kinase that acts to phosphorylate the transcription factor ATF2 [32,33]. In addition, PKA directed phosphorylation of mTORC1/RAPTOR has been shown to mediate a required signal or signals that upregulate UCP1 transcription [34]. Other regulators that are responsive to β-adrenergic stimulation in adipocytes include PGC1a, and PPARα [28,31,35,36]. Chronic activation of this β-adrenergic pathway in adipocytes leads to the upregulation of UCP1 as well as many of the other genes that are also responsive to NRIP1KO [15,17,18,20,22]. Evidence that adipocytes depleted of NRIP1 show increased responsiveness to the effects of β-adrenergic stimulation has also been reported [15,19]. These considerations raise the important mechanistic question whether the cAMP pathway downstream of β-adrenergic signaling is required for and contributes to the upregulation of UCP1 expression induced by NRIP1KO. A related question is what nuclear receptor or receptors are directly repressed by NRIP1 in its role of downregulating thermogenesis? NRIP1 is known to act as a corepressor of many nuclear receptors, and it was shown that ERRα is required for its regulation of glucose transport in adipocytes [18]. ERRα and ERRγ are known to also function in liver and brown fat to enhance whole body glucose metabolism [37,38].

The aim of the present studies was to address these questions on the relationships between NRIP1 signaling and the cAMP and ERRα pathways in mediating the thermogenic response. In addition, we addressed the related question of whether the increased thermogenesis observed in NRIP1KO adipocytes translates into increased energy expenditure in mice after implantation. Our results revealed that 1.) Implantation of NRIP1KO adipocytes into HFD fed mice does upregulate systemic energy expenditure, and 2.) neither upstream (Gsα) nor downstream (PKA) elements of the cAMP signaling pathway are required for the actions of NRIP1KO to upregulate UCP1 and thermogenic genes in adipocytes. Similarly, NRIP1 regulates thermogenesis independently of ERRα.

## 2. MATERIAL AND METHODS

### 2.1. Animals and diets

All animal work was approved by the University of Massachusetts Medical School Institutional Animal Care Use Committee (IACUC protocol no.202200006 to Michael P. Czech). Mice were housed at 20–22 °C on a 12-hour light/12-hour dark cycle with ad libitum access to food and water. C57BL/6J male mice were purchased from Jackson Laboratory for implant studies. C57BL/6J (Jackson Laboratory) male mice were bred for primary preadipocyte cultures. To generate adipocyte-specific Gsα (*Gnas*) knock-out mice that were then used for iWAT SVF (inguinal white adipose tissue stromal vascular fraction) isolation, homozygous Gsα–Flox/Flox animals were crossed to Adiponectin-Cre mice (B6; FVB-Tg (Adipoq-cre)1Evdr/J) as previously described [28,30]. Briefly, 10-week-old male mice arrived and were allowed to acclimate for a week prior to any procedures. Baseline glucose tolerance tests were performed three days before implantation procedures. Mice were implanted under anesthesia with edited primary mouse adipocytes between 10 and 11 weeks of age. Anesthesia was achieved with an anesthesia vaporizer chamber with a continuous flow 500 cc/minute of $0_2$ with 3% (v/v) isoflurane for induction and 1.5% (v/v) for maintenance. After the cell injections, animals were allowed to recover. Mice were maintained on a chow diet for 6 weeks following implantation and then were placed on a 60 kcal% fat diet (Research Diets, D12492i) for the remainder of the study. Glucose tolerance tests were performed after 16-hour overnight fasting with intraperitoneal injection of 1 g/kg D (+) glucose. Insulin tolerance tests (ITTs) were performed with 0.75 IU/kg which did not yield an appropriate response and then with 1 IU/kg after a 6-hour daytime fasting. Additional ITTs with increased insulin dosage could not be performed because of the time-sensitivity of the follow-up of the cohorts. As previously described, body composition was noninvasively measured in mice using 1H-magnetic resonance spectroscopy (Echo-MRI; Echo Medical System). Energy balance was noninvasively assessed with indirect calorimetry for 72 h using metabolic cages (TSE Systems, Inc) [39].

### 2.2. Primary mouse preadipocyte isolation, culture and differentiation to primary adipocytes

3 to 4 week-old C57BL/6J male mice or *Gnas* Flox–Flox or *Gnas* Flox-Adiponectin Cre mice were euthanized and inguinal fat tissue was harvested (including lymph node) and placed in HBSS buffer (Gibco #14025) plus 3% (w/v) bovine serum albumin (BSA) (American Bioanalytical) for SVF isolation and the primary preadipocytes were grown, transfected and differentiated as described previously [15,18]. Briefly, the cells were cultured to sub-confluence in complete media containing DMEM/F12 media (Gibco #11330), 1% (v/v) Penicillin/streptomycin, 10% (v/v) Fetal bovine serum (FBS) (Atlanta Biologicals #S11550), 100 μg/mL Normocin (Invivogen #Ant-nr-1). For cAMP activation, the mature adipocytes were treated with 1 nM (unless otherwise specified) of CL 316,243 disodium salt compound (Tocris Biotechne, Catalog No. 1499) resuspended in $ddH_2O$ following serial dilutions. For 1 mM cAMP treatment, dibutyryl-cAMP sodium salt was purchased (Tocris Biotechne, Catalog No. 1141) and was resuspended in $ddH_2O$ to a concentration of 100 mM. The same volume of $ddH_2O$ was added in the cell cultures as vehicle.

### 2.3. Transfection of primary preadipocytes with ribonucleoprotein (RNP)

For RNP transfection, we used the Neon Transfection System 10 μL or 100 μL Kits (ThermoFisher, #MPK10096) depending on the expected targeted cell population and we prepared a mix consisting unless otherwise specified of sgRNA 4 μM (Synthego or IDT DNA) purified *Spy*Cas9 protein 3 μM (PNA Bio, #CP02) or 3xNLS-SpCas9 [40] (purified by the Scot Wolfe laboratory) in Buffer R provided in the Neon Transfection System Kit. The cells were resuspended in Resuspension

 

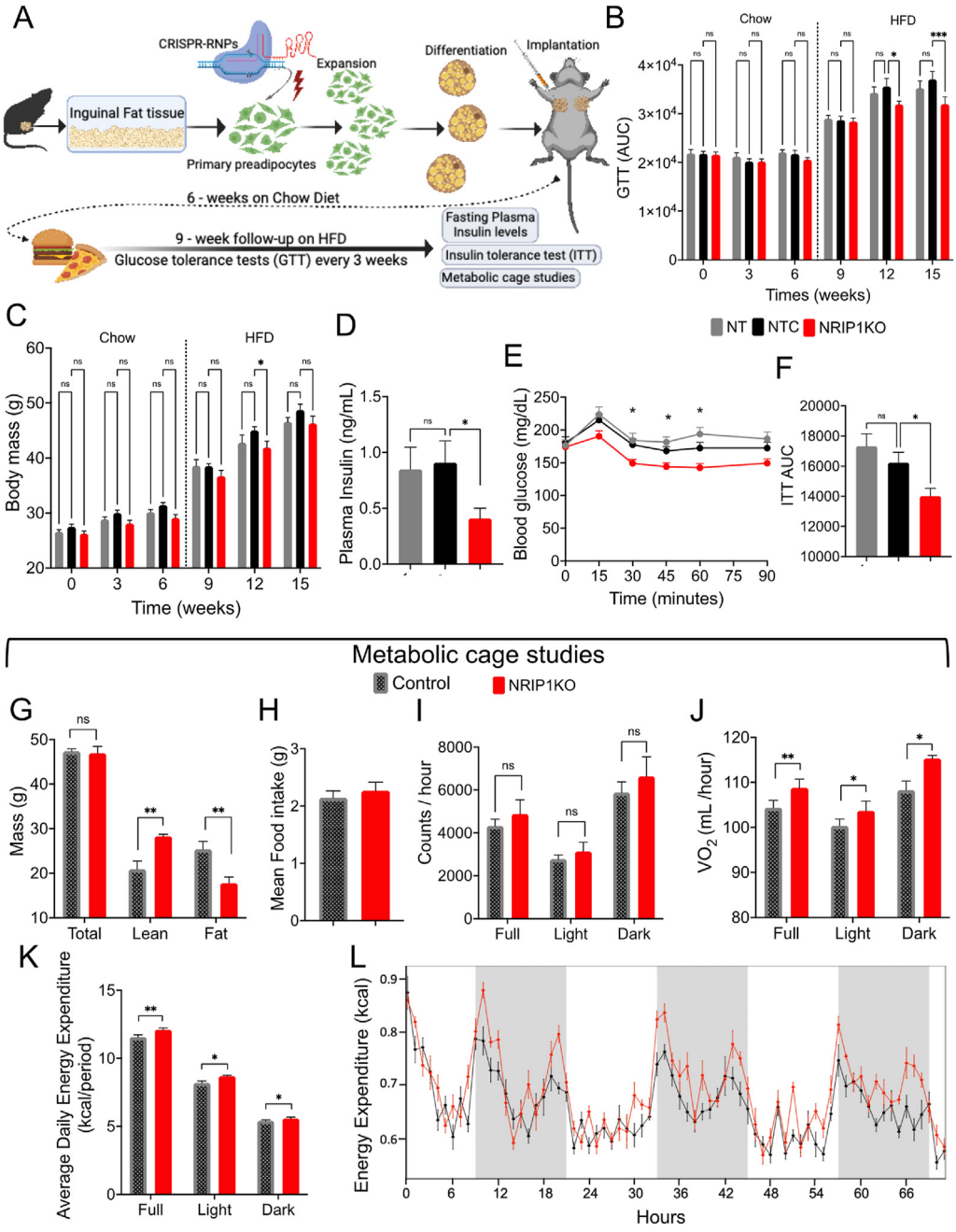


**Figure 1: Mouse NRIP1KO adipocyte implants, unlike control adipocyte implants, improve glucose tolerance, adiposity, insulin sensitivity and increase energy expenditure in recipient mice on fat-enriched diet. A.** Schematic graph and timeline of the cohort study and follow up. **B.** Time-course areas under the curve of glucose tolerance tests with 1 g/kg of D-glucose following a 16-hour overnight fasting in mice without implants (NT), mice with implants of non-targeted control adipocytes (NTC), and in mice with implants of NRIP1KO adipocytes (NRIP1KO). 0 week is the baseline pre-implantation measurement. The dashed line separates the measurements on chow (left) and on high-fat diet (right) **C.** Time-course total body mass follow up of recipient mice. **D.** Plasma insulin measurements following a 16-hour overnight fasting. One value in the NRIP1KO mice was below the detecting point of the assay so it was replaced with the minimum detectable value (0.09). **E.** Insulin tolerance test curves **F.** areas under the curve following a 6-hour daytime fasting with 1IU/kg of insulin administered i.p. in week 16 of study (10 weeks on HFD). **G.** Body composition studies with 1H-MRS at week 16 following implantation in NT and NTC mice (Control) and NRIP1KO implant recipient mice (NRIP1KO). **H.** Average food intake in a three-day metabolic cage study in NT and NTC mice (Control) and NRIP1KO implant recipient mice (NRIP1KO). **I.** Physical activity in a three-day metabolic cage study in NT and NTC mice (Control) and NRIP1KO implant recipient mice (NRIP1KO) full-day, and in the light and dark hours separately. **J.** $O_2$ consumption in a three-day metabolic cage study in NT and NTC mice (Control) and NRIP1KO implant recipient mice (NRIP1KO) full-day, and in the light and dark hours separately. **K.** Average daily energy expenditure in a three-day metabolic cage study in NT and NTC mice (Control) and NRIP1KO implant recipient mice (NRIP1KO) full-day, and in the light and dark hours separately. **L.** Energy expenditure time-point plot during a 72-hour metabolic cage study in NT and NTC mice (Control) and NRIP1KO implant recipient mice (NRIP1KO) full-day, and in the light and dark hours separately. In A-C,E,F, $N^{NT} = 9$, $N^{NTC} = 9$, $N^{NRIP1KO} = 11$. In D, $N^{NT} = 9$, $N^{NTC} = 9$, $N^{NRIP1KO} = 9$. In G-L, $N^{NT} = 3$, $N^{NTC} = 4$, $N^{NRIP1KO} = 5$Bars denote mean and error bars denote mean +S.E.M. In panels B,C,F statistical analysis was performed with 2-way ANOVA multiple comparisons Dunnett's test where each condition was compared to NTC as control. In panel D, and E unpaired 2-tailed t-test was used between NT vs NTC and NTC vs NRIP1KO. In G-I, statistical analysis was performed with unpaired 2-tailed t-test was used between control and NRIP1KO in each condition and in J-K, general linear regression analysis was used via the CalR software with the total body mass used as adjusted covariant. *$p < 0.05$, **$p < 0.01$, ***$p < 0.001$.

 

Buffer R to a final density as suggested by the manufacturer per electroporation. For delivering the RNP complex into primary pre-adipocytes the electroporation parameters used were voltage 1350 V, pulse width 30 ms; number of pulses 1 according to our previous optimization experiments [15]. The electroporated cells were placed in complete media immediately following transfection, expanded, grown to confluence, and differentiated into mature adipocytes for downstream applications. *Nrip1* gene was targeted with sgRNAs 5′ ACAGGCTGTTGCCAGCATGG 3′ and 5′ ATAAGGTTTGGAGTCACGTC 3′ for the implantation and in vitro experiments, respectively. *Esrra* gene was targeted with sgRNA 5′ GATCACCAAGCGGAGACGCA 3'.

### 2.4. Implantation of primary mouse adipocytes

For the implantation of edited adipocytes on day 6 post differentiation, we followed the protocol and procedures previously described [15]. Briefly, the procedure included washing with 1X PBS and dissociation of the cells from the plate using a trypsin-collagenase solution. The detached cells are pelleted at 300 rcf for 10 min at room temperature, washed twice with 1x PBS, then kept on ice for a brief time until implantation. Each pellet deriving from 1 × 150 mm fully confluent plate was mixed with matrigel (Corning® Matrigel® Growth Factor Reduced Basement Membrane Matrix, Phenol Red-free, LDEV-free # 356231) up to a total volume of 500 μL and the cell and matrigel suspension was subcutaneously injected into the anesthetized recipient C57BL/6J mouse using a 20G needle. Each mouse received 2 × 150 mm plates of fully differentiated murine adipocytes in two subscapular, bilateral injections. Figure 1B, and C include but are not limited to glucose tolerance test all time points and body mass data in week 0, 9, 12 and 15 from NTC and NRIP1KO implant recipients that have been previously reported [15], in addition to new data from non − implanted mice and body masses from all groups in week 3 and 6. Due to the inclusion of the third NT group, we now employed 2-way ANOVA for the statistical analysis of these data.

### 2.5. DNA harvest from cells and tissue

At two distinct time-points, 72 h following transfection and after primary adipocyte differentiation (approx. 10−13 days post transfection), genomic DNA was isolated from the transfected cells using DNA QuickExtract™ Buffer (Lucigen) in adherence to the manufacturer's instructions.

### 2.6. Indel analysis by TIDE and ICE

Genomic DNA was PCR amplified for downstream analysis using locus specific primers designed with MacVector 17.0 and purchased from IDT DNA and Genewiz, spanning the region 800 bp around the expected double strand break (DSB). For the PCR amplification, Kappa 2x Hot start HiFi mix was used and PCR products were purified using the Qiagen QIAquick PCR purification kit following the manufacturer's instructions and submitted to Genewiz for Sanger Sequencing. Sanger sequencing trace data were analyzed with TIDE and ICE webtools (http://shinyapps.datacurators.nl/tide/, https://ice.synthego.com/#/) that decipher the composition of indels created at the sites of DSBs [41,42]. All primers used for the assessment of on-target editing are listed in Supplementary Table in the Appendix.

### 2.7. RNA isolation

Transfected cells were harvested for RNA by removing media and washing once with 1xPBS and adding Trizol reagent to lyse the cells. The protocol for RNA isolation was performed according to manufacturer's instruction with the following modifications: 1 μL of Glycol blue (Invitrogen #AM9516) was added to the isopropanol to precipitate the RNA and was stored overnight at −20 °C. The isolated RNA was resuspended in RNase-free water, then treated with recombinant DNase I (DNA-free DNA removal kit, Ambion #1906) according to the manufacturer's instructions. RNA concentrations were determined by Nanodrop 2000.

### 2.8. RT-PCR

For this procedure 1 μg of RNA was used in 20 μL reaction with Bio-Rad iScript cDNA synthesis kit according to manufacturer's instructions for cDNA synthesis. cDNA was diluted up to 100−120 μL with $ddH_2O$ and 5 μL of the diluted cDNA was used as template for RT-PCR with Bio-Rad Sybr Green Mix and gene-specific primers for a final concentration of 0.3 μM primers. Expression of genes was determined with the ΔΔCT method using 36B4 as housekeeping gene. All primers used for RT-PCR are listed in Supplementary Table in the Appendix.

### 2.9. Protein isolation

Adipocytes grown in culture dishes were washed once with 1 x PBS at room temperature, followed by adding boiling 2% SDS (w/v) with 1 X HALT protease inhibitors and scraping to lyse the cells. The cell lysates were sonicated at 60% amplitude with a probe sonicator tip for 10 s at room temperature. Protein concentration of cell lysates was determined using a bicinchoninic acid kit (BCA Protein Assay Kit, Pierce #23227). Protein samples were prepared for western blotting at a final concentration of 1 mg/mL protein, 1x Laemmli loading buffer (BioRad) with 2.5% (v/v) β-Mercaptoethanol, followed by placing in a heat block at 100 °C for 10 min.

### 2.10. Western blotting

Protein lysates were run on 4−15% Gradient Mini-Protean TGX stain-free pre-cast protein gels, followed by transferring the proteins to Nitrocellulose membrane. Unless otherwise stated, a total of 20 μg of protein lysate was loaded per well and nitrocellulose membranes were blocked using 5% (w/v) Non-fat milk in Tris buffered saline with 0.1% (v/v) Tween-20 (TBST) for 4 h at room temperature. Primary antibody incubations were carried out in 5% (w/v) BSA in TBST at the following antibody concentrations: UCP1-Abcam#10983; Anti-pHSL (Ser563) Cell Signaling Technology Cat# 4139; Anti-phospho PKA substrate (RRXS*/T*) Cell Signaling Technology Cat# 9624; ERRa-antibody Cell Signaling Cat# 13826, 1:1000; Vinculin Cell Signaling Technology Cat# 18799, OXPHOS Abcam #110413, Tubulin Sigma Cat# T5168. Blots and primary antibodies were incubated overnight with a roller mixer at 4 °C. Membranes were washed with TBST prior to secondary antibody incubations. HRP-conjugated secondary antibodies were diluted with 5% BSA (w/v) in TBST at 1:10,000 for 45 min at room temperature with constant shaking. Membranes were washed in TBST, followed by incubating with Perkin Elmer Western Lightning Enhance ECL. The Bio-Rad Chemi-Doc XRS was used to image the chemiluminescence and quantifications were performed using the system software, or Image J v.1.51.

### 2.11. Immunofluorescence preparation and imaging

For the immunofluorescence, a previously described protocol was used [43]. Briefly, the cells were seeded on cover slips in the setting of the experiment. At the time-point as specified by the experimental design, the wells were washed with PBS 1X and fixed with 4% (v/v) paraformaldehyde in PBS for 10 min at room temperature. After three short washes with PBS 1X, 100% ice cold methanol was applied for 10 min at 4 °C for permeabilization. After 3 short washes with PBS 1X, normal goat blocking solution was used for blocking for 60 min. The

 

primary antibody incubation (UCP1-Abcam#10983, 1:100; Perilipin 1-ThermoFisher #GT2781, 1:100) was overnight at 4 °C followed by three short washes with PBS 1X and incubation with the secondary antibody Alexa Fluor-594 goat anti-rabbit and Alexa Fluor-488 goat anti-mouse (1:500, Invitrogen) for 1 h at room temperature in the dark. Two washes with PBS 1X were performed and in the last wash, DAPI 1 μg/mL in PBS and was applied on the cells for 5 min to stain the nuclei. The coverslips were mounted in Prolong Gold (Invitrogen) and were allowed to dry overnight prior to imaging. Images were taken with Leica TCS SP8 confocal microscope using LAS-X software and 3—4 randomized z-stacks of 7 images per stack were taken from each condition. The images were analyzed with Fiji/ImageJ2 v. 2.9.0/1.53t and manual blinded cell count was performed by three independent investigators on the same images.

### 2.12. RNA-sequencing

RNA was isolated on day 7 post differentiation after 7 h of stimulation with CL 316,243 or vehicle as described above. The samples underwent DNase treatment, and 2 μg of total RNA was submitted to GENEWIZ for standard RNA sequencing (Illumina HiSeq). The data were acquired demultiplexed in the form of FASTQ files. Alignment and quantification of gene expression levels were performed using the DolphinNext RNA-seq pipeline (revision 6) [44]. Parameters for the pipeline were set to remove Illumina 3' adapter sequences using trimmomatic software (v0.39) with seed mismatches set to 2, a palindrome clip threshold of 30 and a simple clip threshold of 5. The DolphinNext pipeline used RSEM (v1.3.1) to align RNA-Seq reads to a mouse reference transcript (using the RSEM reference STAR and and Bowtie genomes) to estimate gene expression levels. DESeq2 software (v 1.28.1) was then used on these expression levels to find differentially expressed genes between two groups of samples. We set the parameters test = "LRT" (Likelihood Ratio Test), fitType = "parametric", betaPrior = FALSE, and reduced = ~1 (to compare to the control group). padj was set to 0.05 and a minFC = 1.3 was specified. Once differentially expressed genes were found, enriched pathways were identified using the WebGestalt online tool and a p value cut-off of 0.05 [45—49].

### 2.13. Plasma insulin measurements

Whole blood was collected from the mouse recipients from their submandibular vein under anesthesia which was administered as described in 2.1 on week 15 following implantation after an overnight 16-hour fasting. The blood was placed in EDTA containing tubes and the plasma was collected after a 15-minute centrifugation at 2,000 rcf and 4 °C. For insulin measurements, ELISA kit (Crystal Chem) used with 40 μL per sample and the assay was read with a Luminex 200 machine (Millipore). For the data analysis, the measurement found to be below the detectable cut-off, was replaced with 0.09 ng/mL which is the lowest detectable value of 0.09 ng/mL by the kit.

### 2.14. Statistics and reproducibility

For the statistical analysis of the data, GraphPad Prism 9.5.1 was used unless otherwise specified (see 2.12, 2.15) and the statistical methods used for each analysis are described in the corresponding figure legend. The data are presented as means ± S.E.M. p value $< 0.05$ was the threshold for statistical significance.

### 2.15. Databases, software, and online tools

For the mapping of exons on the *Nrip1* and *Esrra* genes we used IGV_2.5.3. For the Design of sgRNAs we used a combination of the Broad Institute sgRNA designer, CHOPCHOP and the online sgRNA checkers by Synthego and IDT. For the design of genomic DNA primers, we used MacVector 17.0. For the statistical analysis and data presentation of the metabolic cage studies we used the CalR app [50—52]. For the design of RT-PCR primers we used Primer Bank (https://pga.mgh.harvard.edu/primerbank/). For the browning probability potential, the unnormalized mapped read counts were applied in the ProFAT online tool [53]. For the transcription factor analysis, the online available software ChEA3 was used [54]. For the data graphing, we used Prism GraphPad 9 unless otherwise specified.

## 3. RESULTS

### 3.1. NRIP1KO adipocytes improve insulin sensitivity, adiposity, and energy expenditure in recipient mice on HFD

To study the systemic metabolic effects of *Nrip1* disruption in adipocytes, we used CRISPR RNP delivery [15] to disrupt *Nrip1* in murine preadipocytes which were then differentiated into mature NRIP1KO or NTC adipocytes, respectively. Recipient mice received implants of NRIP1KO or NTC adipocytes in the subcutaneous subscapular space bilaterally while another age and gender-matched group remained without implants (NT). All mice underwent baseline body mass and fasting glucose tolerance tests prior to randomization and implantation and these measurements were repeated every 3 weeks. Six weeks following implantation, the mice were placed on HFD to induce glucose intolerance and they were followed up for a total of 16 weeks (Figure 1A). While on chow diet, no differences were observed among groups in glucose tolerance. After 6 and 9 weeks on HFD, the NRIP1KO implant recipient mice exhibited significantly improved glucose tolerance compared to the NTC implanted mice and the NT control mice (Figure 1B), consistent with our previous observations [15]. There was a transient decrease in total body mass of the NRIP1KO implanted mice, however, by the end of the follow-up period there were no significant differences in the total body mass (Figure 1C). At 16 weeks after implantation (10 weeks following HFD feeding), fasting plasma insulin of the mice implanted with NRIP1KO adipocytes was significantly lower (Figure 1D) and insulin sensitivity as detected by insulin tolerance tests was improved compared to the control groups with a 14% reduction of the area under the curve (Figure 1E, F). These data are consistent with the concept that implanted NRIP1KO adipocytes confer enhanced insulin sensitivity of liver or skeletal muscle or both. Since there was no weight loss at the end of the study, we suggest that the increased glucose uptake and the secreted factors from the NRIP1KO adipocytes [8,11,15,18] may be the causes of this beneficial effect.

To further examine the physiological effects of the NRIP1KO adipocytes after implantation, we performed metabolic cage studies. Strikingly, despite the absence of total body mass effects, the mice that received NRIP1KO implants had increased lean mass and decreased fat mass without differences in food uptake or physical activity (Figure 1G-I). After a 3-day follow-up, oxygen consumption and energy expenditure were increased in the NRIP1KO implant recipients both during the light and dark cycles (Figures 1J-L). Interestingly, no differences were observed between the NT and the NTC implant recipients (Supplementary Fig. 1), suggesting that the described effects are solely attributable to the consequences of NRIP1 protein depletion in the implanted adipocytes rather than the implants themselves. Taken together, NRIP1KO adipocyte implants protect against development of insulin resistance in response to HFD, increase lean to fat mass ratio and enhance energy expenditure in mice. The mechanisms that mediate these effects are unknown, but NRIP1KO adipocytes

 

themselves show a marked increased uncoupled respiration and energy expenditure [15,17]. Whether this cell autonomous increase in oxygen consumption is enough to contribute to the increase in systemic energy expenditure in NRIP1KO implanted mice is unclear and will be a topic for future investigation.

### 3.2. NRIP1 depletion induces thermogenic programming independent of the cAMP pathway

In murine adipocytes the $\beta_3$-adrenergic receptor in response to agonist CL 316,243 (Figure 2A) acts via the heterotrimeric protein Gs$\alpha,\beta,\gamma$ to activate its effector adenylyl cyclase, producing cAMP from ATP

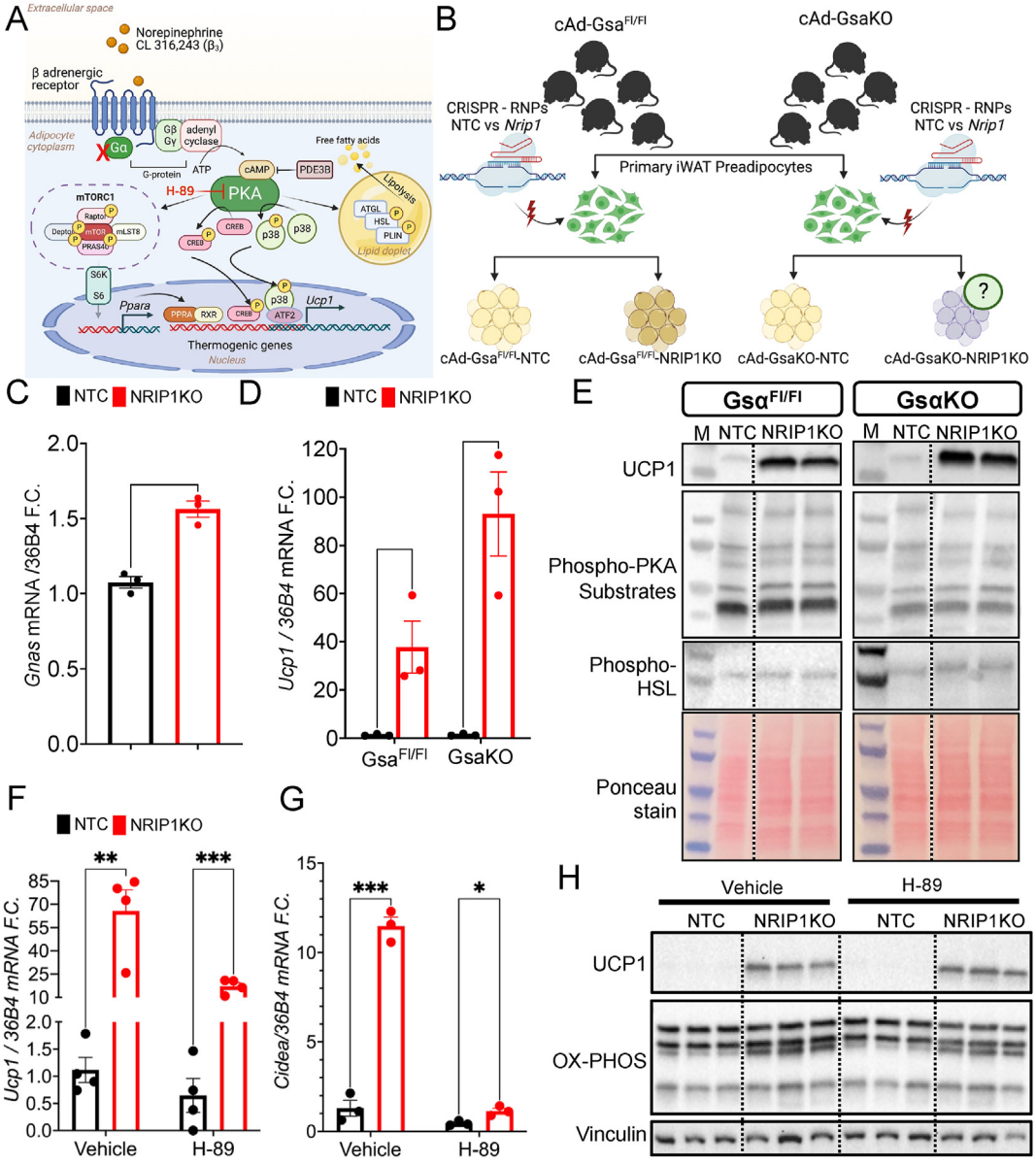


**Figure 2: The adipocyte browning phenotype induced by NRIP1KO *in vitro* is independent of cAMP signaling. A.** cAMP activation by β adrenergic agonists can be blocked by depletion of the GTPase Gsα in adipocytes which is normally activated by endogenous or chemical ligands such as norepinephrine or CL 316,243 (see Introduction and references for details) **B**. Schematic representation of double KO murine primary adipocytes in vitro to explore the phenotype of NRIP1KO in the absence of cAMP activation. **C.** NRIP1 deletion induces a 1.5 folds-change upregulation of Gsα mRNA by RT-PCR. **D.** *Ucp1* mRNA by RT-PCR in primary adipocytes derived from adipose-specific cAdGsa$^{Fl/Fl}$ or cAdGsaKO mice transfected with NTC or *Nrip1* targeting RNPs on day 6 post differentiation. **E.** UCP1 protein, phosphorylated protein kinase A (PKA) substrates, phosphorylated hormone-sensitive lipase (HSL) by western blot in primary adipocytes derived from adipose-specific Gsa$^{Fl/Fl}$ or cAdGsaKO mice transfected with NTC or *Nrip1* targeting RNPs on day 6 post differentiation and ponceau stain of nitrocellulose membrane as loading control. **F.** *Ucp1* and **G.** *Cidea* mRNA by RT-PCR in primary adipocytes mice transfected with NTC or *Nrip1*-targeting RNPs and treated on day 6 post differentiation with vehicle or H-89 for 24 h prior to RNA isolation. **H.** UCP1 protein and oxidative phosphorylation complexes by western blot in primary adipocytes transfected with NTC or *Nrip1* targeting RNPs and treated on day 6 post differentiation with vehicle or H-89 for 24 h prior to protein isolation and vinculin as loading control. Each well is loaded with a sample from an independent experiment. M denotes marker. RT-PCR data normalized over cAdGsa$^{Fl/Fl}$-NTC in panels C, D, and over NTC + Vehicle in panels F, G. Statistical analysis in panel C was performed with paired 2-tailed T-test and in panels D, F, G with multiple unpaired two-tailed T-test. Each circular symbol represents a biological replicate and is the average of the technical replicates of an independent experiment. Bars denote mean and error bars denote mean +/− S.E.M. *$p < 0.05$, **$p < 0.01$, ***$p < 0.001$.

 

[9,27,55,56]. Our RNA sequencing data showed that in *Nrip1*-depleted adipocytes, *Gnas* mRNA encoding Gsα protein is upregulated [15,57] (Supplementary Fig. 2), a finding that was confirmed by RT-PCR (Figure 2C). Based on this data, we investigated the hypothesis that the UCP1 upregulation in response to NRIP1 depletion is partly due to enhancement of the cAMP pathway in adipocytes. To test this hypothesis, we isolated SVF from iWAT of cAdGsaKO mice and cAdGsa$^{Fl/Fl}$ mice. We then transfected the preadipocytes with NTC or *Nrip1* targeting CRISPR RNP to create single and double knock-out cells for NRIP1KO and GsαKO. (Figure 2B, Supplementary Fig. 2). The system was validated by stimulation with CL 316,243 and dibutyryl-cAMP, confirming the lack and presence of PKA substrate phosphorylation and UCP1 response, respectively (Supplementary Fig. 2).

The ablation of the β-adrenergic receptor signaling pathway at the level of Gsα had no effect on the UCP1 upregulation in response to the NRIP1 depletion in the double knock-out cells, which occurred independent of the phosphorylation of PKA substrates, including HSL (Figure 2D, E, Supplementary Fig. 2). To eliminate the possibility that PKA is activated independently of cAMP in response to NRIP1 depletion, we treated NTC and NRIP1KO adipocytes with PKA inhibitor H-89 (Figure 2F–H, Supplementary Fig. 3). No inhibition of the NRIP1KO-induced UCP1 upregulation was observed despite the complete blockade of PKA-induced phosphorylation of substrates by H-89 with or without norepinephrine stimulation (Supplementary Fig. 3). These findings suggest that UCP1 upregulation is independent of the canonical thermogenesis pathway involving cAMP from any source and PKA. These data are compatible with the observation that NRIP1 directly silences *Ucp1* expression via histone modifications leading to methylations on the enhancer [24]. Additionally, NRIP1 likely binds to one or more nuclear receptors, which then control UCP1 expression independent of direct regulation of such factors by PKA.

### 3.3. NRIP1 depletion synergizes with the cAMP pathway to induce UCP1 mRNA expression

Though the thermogenic phenotype associated with NRIP1 depletion is independent of the PKA activity, we tested whether the combination of the two interventions might enhance UCP1 expression more than either alone. To explore this hypothesis, SVF was isolated from wild-type mice and CRISPR was employed to disrupt *Nrip1* prior to inducing adipogenic differentiation. The mature adipocytes were then treated with either vehicle or CL 316,243 for 7 or 24 hours prior to harvesting RNA and protein, respectively (Figure 3A). Strikingly, the *Ucp1* mRNA was synergistically upregulated in the NRIP1KO adipocytes that were treated with the $\beta_3$-adrenergic receptor agonist compared to NRIP1KO alone (Figure 3B). However, at the UCP1 protein level, the effect of the two perturbations was roughly additive (Figure 3C). The phosphorylation of PKA substrates in response to the CL 316,243 treatment was unaffected by the Nrip1 disruption (Figure 3 B, C). These data are consistent with the results in Figure 2 and indicate that the impact of the two perturbations of NRIP1KO and elevated cAMP are independently active when both perturbations are invoked. Overall, these data are also consistent with the established concept that cAMP acts on the UCP1 promoter through regulation of CREB and ATF/PGC1α, distinct from the NRIP1 mode of regulation [31–33,36].

We next examined whether NRIP1 depletion alone or in combination with cAMP stimulation increases the percentage of UCP1-expressing adipocytes. Immunofluorescence microscopy studies showed that NRIP1 depletion greatly increases the amount of UCP1 expressed (Figure 3D), in agreement with the Western blot data. The percentage of detectable UCP1-expressing cells was found to be about 5% in the presence of CL 316,243 alone under the microscopic conditions used in this study. This percent of cells expressing UCP1 increased several fold when NRIP1 was depleted but did not increase further upon CL 316,243 treatment of NRIPKO cells (Figure 3 D, E). RNA-seq studies showed normalized Ucp1 reads were similarly upregulated by CL 316,243 as well as NRIP1 depletion, and the browning probability of the transcriptome signatures were also increased by either perturbation (Figure 3F, Supplementary Fig. 4). Compared to NRIP1KO adipocytes, the combination of NRIP1 depletion and CL 316,243 stimulation significantly upregulated 169 genes and downregulated 160 genes (Figure 3G). Pathway analysis of the differentially expressed genes between the two conditions revealed that the upregulated genes were associated primarily with amino acid turnover pathways, glycolysis, glycogenesis and carbohydrate metabolism while the downregulated genes were associated with several hormonal and non-hormonal signaling pathways and lipolysis (Figure 3H). To further understand which transcription factors may account for the phenotypical differences we observe between NRIP1-depleted adipocytes incubated with or without cAMP stimulation, we used the in silico tool ChEA3 [54]. Among the transcription factors associated with the top 50 upregulated genes are the zinc-finger protein 395 (ZNF395) and C/EBPβ, previously described transcription factors that induce and maintain adipocyte programming in conjunction with PPARγ [58,59]. Other transcription factors known to be downstream of the PKA-cAMP pathway such as CREB5 were also identified. Interestingly, 78 genes associated with PPARγ are found downregulated upon β-adrenergic stimulation of NRIP1KO adipocytes, including C/EBPα that is also known to act in conjunction with PPARγ. Since PPARγ and C/EBPα are known to strongly act synergistically in inducing the adipocyte phenotype, their decreased expressions may indicate a potential negative feedback response opposing browning. This latter finding suggests that manipulation of the system including co-activation of PPARγ along with cAMP increase and NRIP1 depletion could be a powerful approach to increase the thermogenic and metabolically beneficial potential of the NRIP1KO adipocyte implants (Supplementary Fig. 4).

### 3.4. The beiging effects of NRIP1 depletion in adipocytes do not require ERRα

NRIP1 is known to act as a corepressor of many nuclear receptors, including the estrogen receptor related receptors (ERRs) [20]. Indeed, the estrogen related receptor alpha (ERRα) was found to be upregulated upon NRIP1 depletion in a previous transcriptome analysis (Supplementary Fig. 4) [57]. To investigate the extent to which the effects of NRIP1KO on adipocyte beiging are mediated by ERRα, the commonly expressed exon 2/3 of *Esrra* was targeted by CRISPR, coupled with targeting exon 4 in *Nrip1* (Figure 4A). The editing efficiencies at both the *Esrra* and *Nrip1* loci were >90% (Figure 4B, C) without cell toxicity or impairment of the adipogenic differentiation. Following differentiation of the *Esrra*-targeted cells, we found that both the mRNA and ERRα protein in the single KO (*Esrra*-targeted) and in the double KO (DKO = *Esrra* and *Nrip1* -targeted) adipocytes were strongly depleted (Figure 4 D, H). As shown previously, NRIP1KO adipocytes displayed a 1.5-2-fold upregulation of the mRNAs encoding the glucose transporter GLUT4 and the succinate dehydrogenase enzyme (SDHB) [17]. The ERRα depletion significantly downregulated these genes and completely blunted their upregulation upon NRIP1 depletion (Figure 4E, F). Importantly, the ERRα depletion did not affect the elevated UCP1 expression induced by NRIP1KO, which remained at comparable levels

 

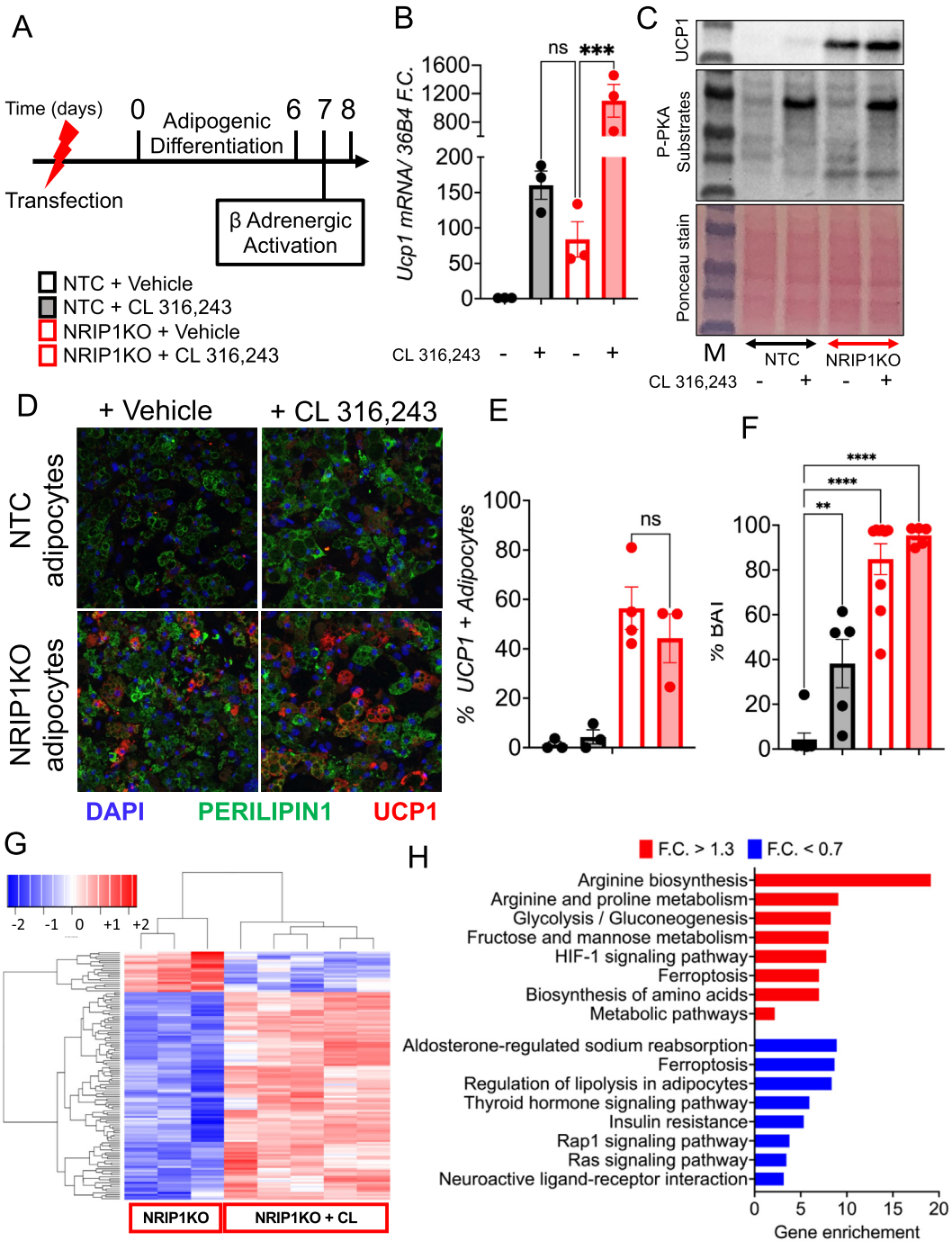


**Figure 3: NRIP1 deletion synergizes with cAMP activation to upregulate UCP1 mRNA levels. A.** Schematic representation of experiment with murine primary preadipocytes transfected with NTC or *Nrip1* targeting RNPs and treated with vehicle or CL 316,243 on day 6 of adipogenic differentiation to activate the cAMP-mediated browning. **B.** *Ucp1* mRNA by RT-PCR in primary adipocytes transfected with NTC or *Nrip1* targeting RNPs and treated on day 6 post differentiation with vehicle or CL 316,243 for 7 h prior to RNA isolation. **C.** UCP1 protein and phosphorylated protein kinase A (PKA) substrates by western blot in primary adipocytes transfected with NTC or *Nrip1* targeting RNPs and treated with vehicle or CL 316,243 on day 6 post differentiation for 24 h prior to protein isolation and ponceau stain of nitrocellulose membrane as loading control. **D.** UCP1 protein detection by immunofluorescence along with co-staining for nuclei and lipid droplets with DAPI and anti-Perilipin antibody in primary adipocytes transfected with NTC or *Nrip1* targeting RNPs and treated with vehicle or CL 316,243 on day 6 post differentiation for 24 h prior to fixing. Magnification is 40X. **E.** Quantification of the UCP1 + cells in immunofluorescence images and calculation of the percentage over all adipocytes in each field. **F.** Browning probability based on RNA sequencing reads in NTC or NRIP1KO primary adipocytes treated with vehicle or CL 316,243 for 7 h prior to total RNA isolation, calculated using the ProFAT online tool. **G.** Heatmap of all differentially expressed genes by RNA-seq between NRIP1KO and NRIP1KO treated with CL 316,243, padj $<0.05$ and F.C. $> 1.3$. **H.** Pathway enrichment analysis of the upregulated (red) and downregulated (blue) genes in the NRIP1KO + CL 316,243 compared to the NRIP1KO + Vehicle adipocytes. M denotes marker. RT-PCR data normalized over NTC + Vehicle. Each circular symbol represents a biological replicate and is the average of the technical replicates of an independent experiment. Statistical analysis was performed by one-way ANOVA and Dunette's multiple comparisons of NRIP1KO + Vehicle with each treatment. Statistical significance of the differential expression in panel G was analyzed as described in the methods section. Bars denote mean and error bars denote mean +/− S.E.M. *$p < 0.05$, **$p < 0.01$, ***$p < 0.001$.

 

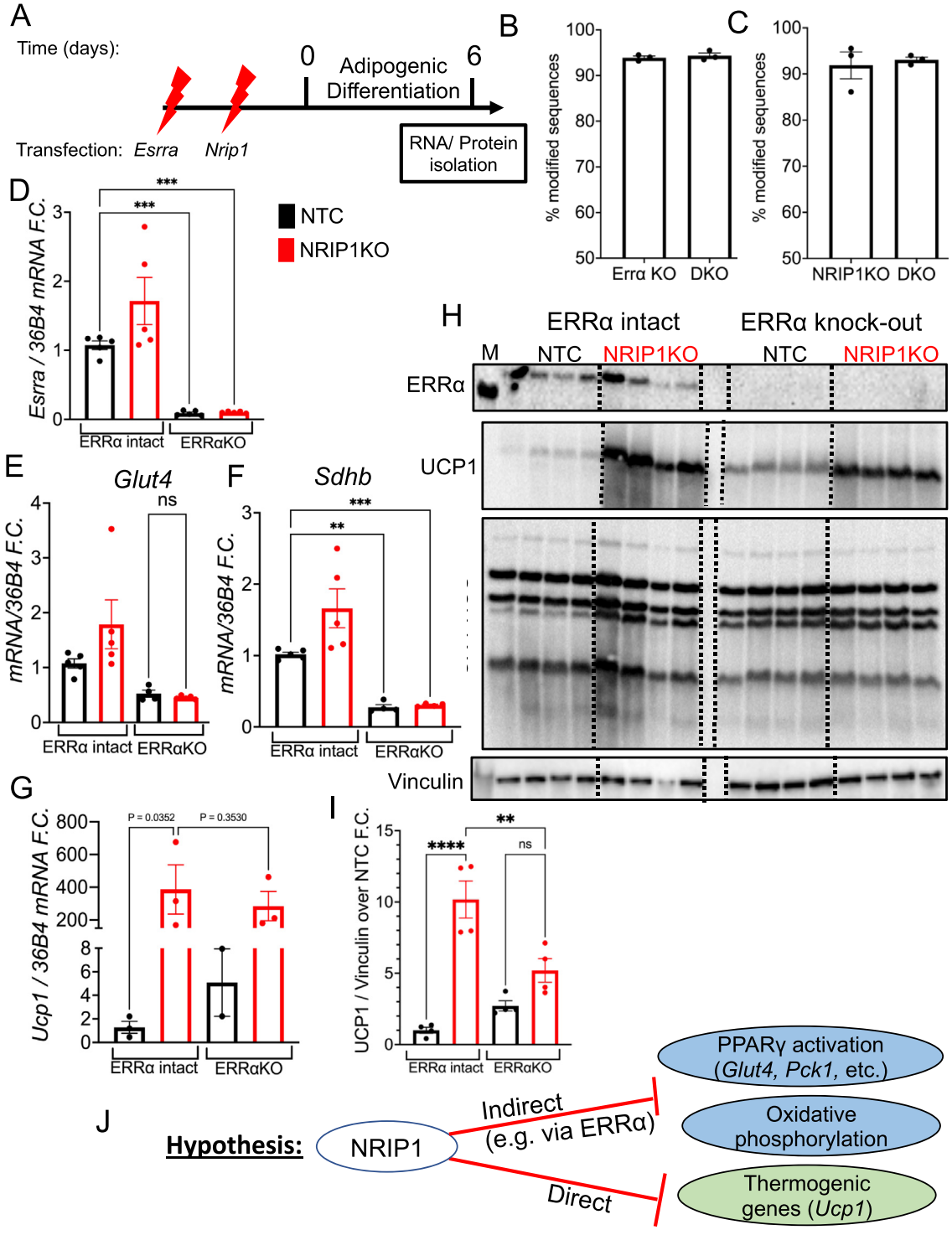


**Figure 4: NRIP1 - mediated UCP1 suppression is independent of ERRα, as opposed to its suppression of Glut4. A.** Schematic representation of the in vitro transfection of murine primary preadipocytes with NTC, *Nrip1,* and *Esrra* targeting RNPs to disrupt *Nrip1, Esrra or Esrra* prior to adipogenic differentiation. **B.** Editing efficiency on *Esrra* coding area by Sanger Sequencing and TIDE/ICE on day 6 following differentiation on ERRαKO and ERRα + NRIP1 double knock-out (DKO) adipocytes. **C.** Editing efficiency on *Nrip1* exon 4 by Sanger Sequencing and TIDE/ICE on day 6 following differentiation on NRIP1KO and ERRα + NRIP1 DKO adipocytes. **D.** *Esrra* mRNA by RT-PCR in the different CRISPR-RNP conditions on day 6 after adipogenic differentiation. **E.** *Glut4,* **F.** *Sdhb* and **G.** *Ucp1* expression by RT-PCR on day 6 after adipogenic differentiation. **H.** ERRα, UCP1 and oxidative phosphorylation complexes (OX-PHOS) protein detection by western blotting on NTC, ERRαKO, NRIP1KO, and ERRα+NRIP1KO adipocytes. Vinculin is used as loading control. **I.** Quantification of UCP1 western blot in Figure 4H. **J.** Hypothesis schematic based on the data showing NRIP1-dependent and NRIP1-independent impacts in adipocyte glucose and energy homeostasis. M denotes marker. Ponceau stain as loading control in the western blotting. Duplicates of representative experiment. Bars denote mean and error bars denote mean +S.E.M. Each circular symbol represents a biological replicate and is the average of the technical replicates of an independent experiment. Statistical analysis was performed by one-way ANOVA and Dunette's multiple comparisons with each treatment. Statistical significance of the differential expression in panel G was analyzed as described in the methods section. Bars denote mean and error bars denote mean +/- S.E.M. *p < 0.05, **p < 0.01, ***p < 0.001.

 

between the NRIP1KO and the NRIP1/ERRα DKO conditions (Figure 4 G—I). However, consistent with this data, the overexpression of oxidative phosphorylation complexes in response to NRIP1KO, was blunted by the disruption of ERRα. These data suggest that ERRα is not required for NRIP1 regulation of UCP1 expression but does mediate the upregulation of oxidative phosphorylation. These data support the hypothesis that NRIP1 depletion enhances adipocyte metabolism and thermogenesis by directly affecting the transcription of thermogenic genes such as Ucp1 but other transcription factors such as ERRα also contribute to this beige-like profile (Figure 4J).

In summary, our data demonstrate the interdependent relationship between the actions of NRIP1KO and the cAMP signaling pathway in controlling UCP1 expression and the thermogenic program of mouse adipocytes. The effect of NRIPKO on UCP1 expression does not require intact signaling of β adrenergic receptors nor of cAMP signaling to PKA. Nor does NRIP1KO require ERRα to upregulate UCP1, as it does to optimally enable insulin stimulation of GLUT4 — mediated glucose transport. However, cAMP signaling strongly adds to the thermogenic effects of NRIP1KO. Future experiments will be necessary to define the nuclear receptors that are the direct targets of NRIP1 in controlling adipocyte thermogenesis.

## APPENDIX

RT-PCR primers.

| RT-PCR Primers | | |
|---|---|---|
| | Forward (5' → 3') | Reverse (5' → 3') |
| *36B4* | TCCAGGCTTTGGGCATCA | CTTTATCAGCTGCACATCACTCAGA |
| *Gnas (Gsa)* | ACAAGCAGGTCTACCGGGCC | CTCCGTTAAACCCATTAACATGCA |
| *Ucp1* | ACTGCCACACCTCCAGTCATT | CTTTGCCTCACTCAGGATTGG |
| *Cidea* | ATCACAACTGGCCTGGTTACG | TACTACCCGGTGTCCATTTCT |
| *Nor-1* | GCTTAAAGGACCAGAGG | TGTCAAGGAAGAGCTTGTCG |
| *Sdhb* | AATTTGCCATTTACCGATGGGA | AGCATCCAACACCATAGGTCC |
| *Glut4* | GTGACTGGAACACTGGTCCTA | CCAGCCACGTTGCATTGTAG |
| *Esrra* | CTCAGCTCTCTACCCAAACGC | CCGCTTGGTGATCTCACACTC |
| Sanger Sequencing primers (sequencing primer in bold) | | |
| | Left (5' → 3') | Right (5' → 3') |
| mNrip1- sgRNA M5 | **CTCTAGGCTGCAGACTGTT** | CAGTGAGTTCTTATAGCTCG |
| mNrip1 -sgRNA M6 | CTCTAGGCTGCAGACTGTT | **CAGTGAGTTCTTATAGCTCG** |
| mEsrra - sgRNA | **CAGTTTGCTATACAGACACC** | GTTTGTACTTCTGCCGTC |
| Genotyping primers [30] | | |

## AUTHOR CONTRIBUTIONS

E.T. and M.P.C. designed the study, interpreted the data and edited the manuscript. E.T. performed most of the experiments, analyzed the data and prepared the manuscript. E.T. and S.M.N. performed the implantations. M.K. established the colonies for mouse cell donors and performed the blood collections of the recipient mice. A.G., K.B.S. and N.W. performed the breeding of Gsa-Flox mice and the genotyping. H.W., K.M., L.R., L.M.L. performed experiments. L.M.L. and E.T. analyzed the RNA-seq data. S.A.M. and S.A.W. purified SpyCas9 protein. R.H.F., and J.K.K. performed the measurement of plasma insulin and metabolic cage studies. M.C. and L.S.W. designed and provided the Gsa Flox mouse model used in the research. All authors reviewed and were invited to edit the manuscript.

## DECLARATION OF COMPETING INTEREST

The authors declare the following competing Interests: M.P.C. and A.G. are inventors of granted US Patent US-8519118-B2, "RIP140 regulation of glucose transport", and of granted US Patent US-8093223-B2, "RIP140 regulation of diabetes", related to data in this manuscript on Nrip1/RIP140-depleted mouse and human adipocytes. M.P.C., E.T., and S.M.N. are inventors of US Patent US-20220220461-A1 and PCT WO2022076812A3, "Targeting Nrip1 to Alleviate Metabolic Disease", related to CRISPR-based depletion of NRIP1 in mouse adipocytes in this manuscript. The University of Massachusetts is the grantee or potential grantee of all the above. M.P.C. declares that he is bound by a confidentiality agreement that prevents him from disclosing a potentially competing interest in this work. S.A.W. is a consultant for Chroma Medicine. The remaining authors declare no competing interests.

## DATA AVAILABILITY

Data will be made available on request.

## ACKNOWLEDGEMENTS

We wish to thank members of the Czech laboratory for helpful discussions and Kerri Miller for excellent assistance in preparing the manuscript. We thank visiting student Ioannis Stouras for the helpful discussions. We also thank the Theuerkauf laboratory at UMass Chan Medical School, Program in Molecular Medicine for access to and assistance with the confocal microscope. This work was supported by the Assistant Secretary of Defense for Health Affairs endorsed by the Department of Defense, through the Peer Reviewed Medical Research Program under Award No. W81XWH-18-1-0398 and W81XWH-21-1-0565 (to M.P.C.). Opinions, interpretations, conclusions, and recommendations are those of the authors and are not necessarily endorsed by the Department of Defense. This work was also supported by National Institutes of Health grants DK130852 (to M.P.C.), HL120669 (to S.A.W.), TR002668 (to S.A.W.), the National Mouse Metabolic Phenotyping Center (MMPC) at UMass Medical School (NIH grant 5U2C-DK093000 to J.K.K.) and the Intramural Research Program of NIDDK, NIH (M.C., L.S.W.). We also gratefully acknowledge generous funding through the Isadore and Fannie Foxman Chair in Medical Science (to M.P.C.). Multiple figures in this manuscript (Figure 1A, Figure 2A,B) were created with Biorender.com.

## APPENDIX A. SUPPLEMENTARY DATA

Supplementary data to this article can be found online at https://doi.org/10.1016/j.molmet.2023.101780.

## REFERENCES

[1] Finck AV, Blanchard T, Roselle CP, Golinelli G, June CH. Engineered cellular immunotherapies in cancer and beyond. Nat Med 2022;28:678—89. https://doi.org/10.1038/s41591-022-01765-8.

[2] Kean LS. Defining success with cellular therapeutics: the current landscape for clinical end point and toxicity analysis. Blood 2018;131:2630—9. https://doi.org/10.1182/blood-2018-02-785881.

[3] Pittenger MF, Discher DE, Peault BM, Phinney DG, Hare JM, Caplan AI. Mesenchymal stem cell perspective: cell biology to clinical progress. NPJ Regen Med 2019;4:22. https://doi.org/10.1038/s41536-019-0083-6.

[4] Rosenberg SA, Restifo NP. Adoptive cell transfer as personalized immunotherapy for human cancer. Science 2015;348:62—8. https://doi.org/10.1126/science.aaa4967.

 

[5] Czech MP. Insulin action and resistance in obesity and type 2 diabetes. Nat Med 2017;23:804—14. https://doi.org/10.1038/nm.4350.
[6] Czech MP. Mechanisms of insulin resistance related to white, beige, and brown adipocytes. Mol Metabol 2020;34:27—42. https://doi.org/10.1016/j.molmet.2019.12.014.
[7] Kusminski CM, Bickel PE, Scherer PE. Targeting adipose tissue in the treatment of obesity-associated diabetes. Nat Rev Drug Discov 2016;15:639—60. https://doi.org/10.1038/nrd.2016.75.
[8] Ahmad B, Vohra MS, Saleemi MA, Serpell CJ, Fong IL, Wong EH. Brown/Beige adipose tissues and the emerging role of their secretory factors in improving metabolic health: the batokines. Biochimie 2021;184:26—39. https://doi.org/10.1016/j.biochi.2021.01.015.
[9] Guilherme A, Rowland LA, Wang H, Czech MP. The adipocyte supersystem of insulin and cAMP signaling. Trends Cell Biol 2023;33:340—54. https://doi.org/10.1016/j.tcb.2022.07.009.
[10] Kajimura S, Saito M. A new era in brown adipose tissue biology: molecular control of brown fat development and energy homeostasis. Annu Rev Physiol 2014;76:225—49. https://doi.org/10.1146/annurev-physiol-021113-170252.
[11] Yang FT, Stanford KI. Batokines: mediators of inter-tissue communication (a mini-review). Curr Obes Rep 2022;11:1—9. https://doi.org/10.1007/s13679-021-00465-7.
[12] White JD, Dewal RS, Stanford KI. The beneficial effects of brown adipose tissue transplantation. Mol Aspect Med 2019;68:74—81. https://doi.org/10.1016/j.mam.2019.06.004.
[13] Stanford KI, Middelbeek RJ, Townsend KL, An D, Nygaard EB, Hitchcox KM, et al. Brown adipose tissue regulates glucose homeostasis and insulin sensitivity. J Clin Invest 2013;123:215—23. https://doi.org/10.1172/JCI62308.
[14] Stanford KI, Goodyear LJ. The therapeutic potential of brown adipose tissue. Hepatobiliary Surg Nutr 2013;2:286—7. https://doi.org/10.3978/j.issn.2304-3881.2013.09.02.
[15] Tsagkaraki E, Nicoloro SM, DeSouza T, Solivan-Rivera J, Desai A, Lifshitz LM, et al. CRISPR-enhanced human adipocyte browning as cell therapy for metabolic disease. Nat Commun 2021;12:6931. https://doi.org/10.1038/s41467-021-27190-y.
[16] Wang CH, Lundh M, Fu A, Kriszt R, Huang TL, Lynes MD, et al. CRISPR-engineered human brown-like adipocytes prevent diet-induced obesity and ameliorate metabolic syndrome in mice. Sci Transl Med 2020;12. https://doi.org/10.1126/scitranslmed.aaz8664.
[17] Powelka AM, Seth A, Virbasius JV, Kiskinis E, Nicoloro SM, Guilherme A, et al. Suppression of oxidative metabolism and mitochondrial biogenesis by the transcriptional corepressor RIP140 in mouse adipocytes. J Clin Invest 2006;116:125—36. https://doi.org/10.1172/JCI26040.
[18] Shen Y, Cohen JL, Nicoloro SM, Kelly M, Yenilmez B, Henriques F, et al. CRISPR-delivery particles targeting nuclear receptor-interacting protein 1 (Nrip1) in adipose cells to enhance energy expenditure. J Biol Chem 2018;293:17291—305. https://doi.org/10.1074/jbc.RA118.004554.
[19] Peppler WT, Miotto PM, Holloway GP, Wright DC. CL 316, 243 mediated reductions in blood glucose are enhanced in RIP140(-/-) mice independent of alterations in lipolysis. Biochem Biophys Res Commun 2017;486:486—91. https://doi.org/10.1016/j.bbrc.2017.03.067.
[20] Nautiyal J, Christian M, Parker MG. Distinct functions for RIP140 in development, inflammation, and metabolism. Trends Endocrinol Metab 2013;24:451—9. https://doi.org/10.1016/j.tem.2013.05.001.
[21] Parker M, White R, Leonardsson G, Milligan S, Steel J. Identification of RIP140 as a nuclear receptor cofactor with a role in female reproduction. Ernst Schering Res Found Workshop 2004:23—31. https://doi.org/10.1007/978-3-662-05386-7_2.
[22] Leonardsson G, Steel JH, Christian M, Pocock V, Milligan S, Bell J, et al. Nuclear receptor corepressor RIP140 regulates fat accumulation. Proc Natl Acad Sci U S A 2004;101:8437—42. https://doi.org/10.1073/pnas.0401013101.
[23] L'Horset F, Dauvois S, Heery DM, Cavailles V, Parker MG. RIP-140 interacts with multiple nuclear receptors by means of two distinct sites. Mol Cell Biol 1996;16:6029—36. https://doi.org/10.1128/MCB.16.11.6029.
[24] Kiskinis E, Hallberg M, Christian M, Olofsson M, Dilworth SM, White R, et al. RIP140 directs histone and DNA methylation to silence Ucp1 expression in white adipocytes. EMBO J 2007;26:4831—40. https://doi.org/10.1038/sj.emboj.7601908.
[25] Solivan-Rivera J, Yang Loureiro Z, DeSouza T, Desai A, Pallat S, Yang Q, et al. A neurogenic signature involving monoamine Oxidase-A controls human thermogenic adipose tissue development. Elife 2022;11. https://doi.org/10.7554/eLife.78945.
[26] Min SY, Kady J, Nam M, Rojas-Rodriguez R, Berkenwald A, Kim JH, et al. Human 'brite/beige' adipocytes develop from capillary networks, and their implantation improves metabolic homeostasis in mice. Nat Med 2016;22:312—8. https://doi.org/10.1038/nm.4031.
[27] Cero C, Lea HJ, Zhu KY, Shamsi F, Tseng YH, Cypess AM. beta3-Adrenergic receptors regulate human brown/beige adipocyte lipolysis and thermogenesis. JCI Insight 2021;6. https://doi.org/10.1172/jci.insight.139160.
[28] Guilherme A, Yenilmez B, Bedard AH, Henriques F, Liu D, Lee A, et al. Control of adipocyte thermogenesis and lipogenesis through beta3-adrenergic and thyroid hormone signal integration. Cell Rep 2020;31:107598. https://doi.org/10.1016/j.celrep.2020.107598.
[29] Cannon B, Nedergaard J. Brown adipose tissue: function and physiological significance. Physiol Rev 2004;84:277—359. https://doi.org/10.1152/physrev.00015.2003.
[30] Li YQ, Shrestha YB, Chen M, Chanturiya T, Gavrilova O, Weinstein LS. Gsalpha deficiency in adipose tissue improves glucose metabolism and insulin sensitivity without an effect on body weight. Proc Natl Acad Sci U S A 2016;113:446—51. https://doi.org/10.1073/pnas.1517142113.
[31] Collins S. Beta-adrenoceptor signaling networks in adipocytes for recruiting stored fat and energy expenditure. Front Endocrinol (Lausanne) 2011;2:102. https://doi.org/10.3389/fendo.2011.00102.
[32] Cao W, Medvedev AV, Daniel KW, Collins S. beta-Adrenergic activation of p38 MAP kinase in adipocytes: cAMP induction of the uncoupling protein 1 (UCP1) gene requires p38 MAP kinase. J Biol Chem 2001;276:27077—82. https://doi.org/10.1074/jbc.M101049200.
[33] Cao W, Daniel KW, Robidoux J, Puigserver P, Medvedev AV, Bai X, et al. p38 mitogen-activated protein kinase is the central regulator of cyclic AMP-dependent transcription of the brown fat uncoupling protein 1 gene. Mol Cell Biol 2004;24:3057—67. https://doi.org/10.1128/MCB.24.7.3057-3067.2004.
[34] Liu D, Bordicchia M, Zhang C, Fang H, Wei W, Li JL, et al. Activation of mTORC1 is essential for beta-adrenergic stimulation of adipose browning. J Clin Invest 2016;126:1704—16. https://doi.org/10.1172/JCI83532.
[35] Yehuda-Shnaidman E, Buehrer B, Pi J, Kumar N, Collins S. Acute stimulation of white adipocyte respiration by PKA-induced lipolysis. Diabetes 2010;59:2474—83. https://doi.org/10.2337/db10-0245.
[36] Collins S, Surwit RS. The beta-adrenergic receptors and the control of adipose tissue metabolism and thermogenesis. Recent Prog Horm Res 2001;56:309—28. https://doi.org/10.1210/rp.56.1.309.
[37] Xia H, Dufour CR, Giguere V. ERRalpha as a bridge between transcription and function: role in liver metabolism and disease. Front Endocrinol (Lausanne) 2019;10:206. https://doi.org/10.3389/fendo.2019.00206.
[38] Ahmadian M, Liu S, Reilly SM, Hah N, Fan W, Yoshihara E, et al. ERRgamma preserves Brown fat innate thermogenic activity. Cell Rep 2018;22:2849—59. https://doi.org/10.1016/j.celrep.2018.02.061.
[39] Dagdeviren S, Jung DY, Lee E, Friedline RH, Noh HL, Kim JH, et al. Altered interleukin-10 signaling in skeletal muscle regulates obesity-mediated inflammation and insulin resistance. Mol Cell Biol 2016;36:2956—66. https://doi.org/10.1128/MCB.00181-16.

 

[40] Wu Y, Zeng J, Roscoe BP, Liu P, Yao Q, Lazzarotto CR, et al. Highly efficient therapeutic gene editing of human hematopoietic stem cells. Nat Med 2019;25:776–83. https://doi.org/10.1038/s41591-019-0401-y.

[41] Brinkman EK, Chen T, Amendola M, van Steensel B. Easy quantitative assessment of genome editing by sequence trace decomposition. Nucleic Acids Res 2014;42:e168. https://doi.org/10.1093/nar/gku936.

[42] Conant D, Hsiau T, Rossi N, Oki J, Maures T, Waite K, et al. Inference of CRISPR edits from sanger trace data. CRISPR J 2022;5:123–30. https://doi.org/10.1089/crispr.2021.0113.

[43] Rowland LA, Guilherme A, Henriques F, DiMarzio C, Munroe S, Wetoska N, et al. De novo lipogenesis fuels adipocyte autophagosome and lysosome membrane dynamics. Nat Commun 2023;14:1362. https://doi.org/10.1038/s41467-023-37016-8.

[44] Yukselen O, Turkyilmaz O, Ozturk AR, Garber M, Kucukural A. DolphinNext: a distributed data processing platform for high throughput genomics. BMC Genom 2020;21:310. https://doi.org/10.1186/s12864-020-6714-x.

[45] Liao Y, Wang J, Jaehnig EJ, Shi Z, Zhang B. WebGestalt 2019: gene set analysis toolkit with revamped UIs and APIs. Nucleic Acids Res 2019;47:W199–205. https://doi.org/10.1093/nar/gkz401.

[46] Wang J, Vasaikar S, Shi Z, Greer M, Zhang B. WebGestalt 2017: a more comprehensive, powerful, flexible and interactive gene set enrichment analysis toolkit. Nucleic Acids Res 2017;45:W130–7. https://doi.org/10.1093/nar/gkx356.

[47] Kirov S, Ji R, Wang J, Zhang B. Functional annotation of differentially regulated gene set using WebGestalt: a gene set predictive of response to ipilimumab in tumor biopsies. Methods Mol Biol 2014;1101:31–42. https://doi.org/10.1007/978-1-62703-721-1_3.

[48] Wang J, Duncan D, Shi Z, Zhang B. WEB-Based GEne SeT AnaLysis toolkit (WebGestalt): update 2013. Nucleic Acids Res 2013;41:W77–83. https://doi.org/10.1093/nar/gkt439.

[49] Zhang B, Kirov S, Snoddy J. WebGestalt: an integrated system for exploring gene sets in various biological contexts. Nucleic Acids Res 2005;33:W741–8. https://doi.org/10.1093/nar/gki475.

[50] Mina AI, LeClair RA, LeClair KB, Cohen DE, Lantier L, Banks AS. CalR: a web-based analysis tool for indirect calorimetry experiments. Cell Metab 2018;28:656–666 e651. https://doi.org/10.1016/j.cmet.2018.06.019.

[51] Corrigan JK, Ramachandran D, He Y, Palmer CJ, Jurczak MJ, Chen R, et al. A big-data approach to understanding metabolic rate and response to obesity in laboratory mice. Elife 2020;9. https://doi.org/10.7554/eLife.53560.

[52] Cortopassi MD, Ramachandran D, Rubio WB, Hochbaum D, Sabatini BL, Banks AS. Analysis of thermogenesis experiments with CalR. Methods Mol Biol 2022;2448:43–72. https://doi.org/10.1007/978-1-0716-2087-8_3.

[53] Cheng Y, Jiang L, Keipert S, Zhang S, Hauser A, Graf E, et al. Prediction of adipose browning capacity by systematic integration of transcriptional profiles. Cell Rep 2018;23:3112–25. https://doi.org/10.1016/j.celrep.2018.05.021.

[54] Keenan AB, Torre D, Lachmann A, Leong AK, Wojciechowicz ML, Utti V, et al. ChEA3: transcription factor enrichment analysis by orthogonal omics integration. Nucleic Acids Res 2019;47:W212–24. https://doi.org/10.1093/nar/gkz446.

[55] Calebiro D, Nikolaev VO, Persani L, Lohse MJ. Signaling by internalized G-protein-coupled receptors. Trends Pharmacol Sci 2010;31:221–8. https://doi.org/10.1016/j.tips.2010.02.002.

[56] Calebiro D, Nikolaev VO, Lohse MJ. Imaging of persistent cAMP signaling by internalized G protein-coupled receptors. J Mol Endocrinol 2010;45:1–8. https://doi.org/10.1677/JME-10-0014.

[57] UMMS. CRISPR-enhanced human adipocyte browning as cell therapy for metabolic disease. 2021.

[58] Hasegawa R, Tomaru Y, de Hoon M, Suzuki H, Hayashizaki Y, Shin JW. Identification of ZNF395 as a novel modulator of adipogenesis. Exp Cell Res 2013;319:68–76. https://doi.org/10.1016/j.yexcr.2012.11.003.

[59] Cristancho AG, Lazar MA. Forming functional fat: a growing understanding of adipocyte differentiation. Nat Rev Mol Cell Biol 2011;12:722–34. https://doi.org/10.1038/nrm3198.

 